OPEN ACCESS
IOP Publishing
Journal of Physics: Condensed Matter
J. Phys.: Condens. Matter **51** (2023) 025703 (8pp)
https://doi.org/10.1088/1361-648X/ac9f94

Tunable anomalous Hall and Nernst effects in MM′X compounds

Ilias Samathrakis*, **Nuno Fortunato, Harish K Singh, Chen Shen and Hongbin Zhang**

Institute of Materials Science, TU Darmstadt, 64287 Darmstadt, Germany

E-mail: iliassam@tmm.tu-darmstadt.de

Received 12 July 2022, revised 26 October 2022
Accepted for publication 1 November 2022
Published 11 November 2022

Abstract

Based on first-principles calculations, the anomalous Hall conductivity (AHC) and anomalous Nernst conductivities (ANCs) of the XMnP (X = Ti, Zr, Hf) compounds are evaluated, and the possibility to tailor such properties in compounds susceptible to changing the magnetization directions is also investigated. We observe large changes in the calculated AHC and ANC for different magnetization directions that are originating from changes in the band structure all over the whole Brillouin zone. Our study gives a promising clue on engineering magnetic intermetallic compounds for tunable transverse thermoelectric applications.

Supplementary material for this article is available online

Keywords: anomalous Hall conductivity, anomalous Nernst conductivity, Berry curvature, topological transport properties

(Some figures may appear in colour only in the online journal)

1. Introduction

The anomalous Hall effect (AHE) describes the generation of a transversal current, perpendicular to the electric field, in the absence of an external magnetic field [1, 2]. Its thermal counterpart, dubbed anomalous Nernst effect (ANE) [3, 4], is achieved if the electric field is replaced by a thermal gradient. Ferromagnetic materials were the first observed to possess non zero AHE and ANE. It was later found that antiferromagnetic materials with noncollinear structure can exhibit large anomalous Hall conductivity (AHC) and anomalous Nernst conductivities (ANCs) with the most representative examples being the Mn_3X with X = (Ge,Ga,Sn,Rh,In) [5–15] and the Mn_3XN with X = (Ga,Zn,Ag,Ni) [16–18] families. Very recently, it was proposed that the collinear antiferromagnet RuO_2 can induce nonzero AHC [19]. The existence of such topological properties in these magnetic materials can be traced back to the appearance of Weyl nodes and nodal lines to the electronic structure [9], being non-accidental linear touching points (Weyl semimetals) or lines (nodal semimetals) close to the Fermi energy, that cause non zero Berry curvature, acting as a fictitious magnetic field, leading to non vanishing effects. From the practical point of view, compounds with large values of AHC and ANC are promising candidates for data storage [20] and data transfer [21] devices that can lead to further spintronics applications.

The MM′X (X = main group element, M and M′ = metal) are a widespread class of compounds that can form in orthorhombic TiNiSi, along with the less common Ni_2In and LiGaGe hexagonal structures. They accumulate several intriguing properties such as the martensitic transition [22–24] and have attracted scientific attention due to interesting properties such as magnetoresistance [25, 26], magneto-strain

* Author to whom any correspondence should be addressed.

effect [27–29] and magnetocaloric effect [30–33], making them promising candidates for solid-state magnetic cooling applications [34–36]. Besides, the members of the MM′X family have been reported to host large AHC and (ANC), such as the primordial research on their topological properties of ZrMnP and HfMnP compounds, showing large AHC values of the order of 1000 S cm^{-1} and 1500 S cm^{-1} respectively [37], due to the presence of nodal lines, rendering them as promising materials [38]. It is noted that the AHC is parsed in intrinsic and extrinsic contributions, the latter of which is further decomposed in side jump and skew scattering. From the theoretical perspective, the side jump contribution is calculated following the procedure described in [39] while that of skew scattering in [40]. More insights on the experimental procedure of determining both the intrinsic and the extrinsic contribution can be found in [41]. Non negligible extrinsic contributions of 1100 S cm^{-1} and 1440 S cm^{-1} have been measured for HfMnP and ZrMnP respectively [37]

In this work, we applied first principles calculations to evaluate the intrinsic part of AHC and ANC of XMnP (X = Ti,Zr,Hf) compounds and altered the magnetization direction to tune such transport properties. Our results demonstrated that both AHC and ANC originated from the combination of nodal lines and small gap areas present in the whole Brillouin zone. It was further observed that the magnetization direction significantly affected the evaluated AHC and ANC with their differences being distributed throughout the whole Brillouin zone

2. Numerical details

Our first principle calculations were performed using the projector augmented wave method, as implemented in VASP software [42]. The exchange-correlation functional was approximated using the generalized gradient approximation as parameterized by Perdew–Burke–Ernzerhof [43]. A Γ-centered kmesh sampling of density 50 in respect to all lattice dimensions as well as an energy cutoff of 500 eV were used. Spin orbit coupling was included in all calculations. The DFT-Bloch wave functions were projected on maximally localized Wannier functions, using the wannier90 software [44]. The MLWFs were constructed for *spd*-orbitals of Mn, Ti and Hf, *sp*-orbitals of *spd*-orbitals of Zr, generated on a kmesh of 40 and the frozen window was computed based on the partial density of states, according to the methodology described in [45]. The AHC was evaluated using Wanniertools [46] by integrating the Berry curvature according to the formula:

$$\sigma_{ij} = \frac{e^2}{\hbar}\int \frac{d\mathbf{k}}{(2\pi)^3}\sum_n f\left[\epsilon\left(\mathbf{k}\right)-\mu\right]\Omega_{n,ij}\left(\mathbf{k}\right), \tag{1}$$

$$\Omega_{n,ij}\left(\mathbf{k}\right) = -2Im\sum_{m\neq n}\frac{\langle \mathbf{k}n|u_i|\mathbf{k}m\rangle\langle \mathbf{k}m|u_j|\mathbf{k}n\rangle}{\left[\epsilon_m\left(\mathbf{k}\right)-\epsilon_n\left(\mathbf{k}\right)\right]^2} \tag{2}$$

where f is the Fermi distribution function, μ the Fermi energy, n and m the occupied and empty Bloch band with $\epsilon_n\left(\mathbf{k}\right)$ and $\epsilon_m\left(\mathbf{k}\right)$ being their energy eigenvalues and v_i the velocity operator. The ANC was computed using an in-house developed python script based on the formula [47]:

$$\alpha_{ij} = -\frac{1}{e}\int d\epsilon \frac{\partial f}{\partial \mu}\sigma_{ij}\left(\epsilon\right)\frac{\epsilon-\mu}{T} \tag{3}$$

where e is the charge of the electron, T the temperature and ε the energy point within an energy grid of 1000 points at a range $\left[-0.5, 0.5\right]$ eV in respect to the Fermi energy.

3. Results and discussion

The transition metal pnictides under consideration crystallize in the orthorhombic *Pnma* (No. 62) space group with lattice parameters being equal to $a = 6.43$ Å, $b = 3.63$ Å, $c = 7.51$ Å for ZrMnP and $a = 6.37$ Å, $b = 3.60$ Å, $c = 7.45$ Å for HfMnP and $a = 6.15$ Å, $b = 3.47$ Å, $c = 7.20$ Å for TiMnP. The lattice constants of all compounds were obtained from high throughput calculations. The values obtained for the former two, agrees with the x-rays experiments in [37, 38]. The magnetic moments originate exclusively from Mn atoms and have been calculated to be $1.74\mu_B$, $2.06\mu_B$ and $1.95\mu_B$ for TiMnP, ZrMnP and HfMnP respectively, in reasonable agreement with the values of $1.8\mu_B$ and $2.0\mu_B$ at $T = 2$K for ZrMnP and HfMnP respectively, calculated in [37]. The input values of the lattice constants and the magnetic moments of Mn atoms are summarized in the table 1. Our DFT calculations were performed on two magnetic configurations, namely with magnetic moments aligned along [100]- and along [001]-axis, as illustrated in figure 1. Changes in the band structure due to magnetization direction is illustrated in figure S1 of supplementary. These two discrepant energetically distinguishable magnetic configurations exhibit a magneticrystalline anisotropy energy of 0.165 meV per Mn atom and 0.43 meV per Mn atom in favor of [100]-direction for ZrMnP and HfMnP respectively. Our results are in good agreement with the values of 0.136 meV per Mn atom and 0.47 meV per Mn atom reported in [38] for ZrMnP and HfMnP respectively, where from the applications point of view, altering the magnetization direction is possible by means of externally applied magnetic field [48], spin orbit torque [49], spin transfer torque [50] and other mechanisms [51]. Recent studies demonstrate that the anisotropic fields required to switch the magnetization directions from the hard [001]-axis to easy [100]-axis in (Zr,Hf)MnP have been calculated to be 4.6 T and 10 T respectively [38], making them within the current experimental capabilities [52]. It is further noted that since the magnetiocrystalline anisotropy of TiMnP, being 0.05 meV per Mn atom, is substantially lower than that of HfMnP and that of ZrMnP (0.43 meV and 0.165 meV per Mn atom respectively), a smaller anisotropic field is expected to be sufficient to control the magnetization directions.

Significant changes in AHC and ANC values are observed by altering the magnetization direction of the system. A schematic illustration of a thermopile is shown in figure 2. The direction of the induced ANC is depicted for fixed directions of thermal gradient, magnetization and electric current. The

Table 1. Summary of lattice constants used as input to our calculations and calculated output of magnetization, AHC, ANC and T_cs compared to the existing literature for TiMnP, ZrMnP, HfMnP.

Compound	Lattice constant (Å)			Magnetization (μ_B)		AHC (S cm^{-1})			ANC (A mK^{-1})		Curie temp.
	a	b	c	Calculated	Theory	$\sigma_x, M\|\|[100]$	σ_x (theory)	$\sigma_z, M\|\|[001]$	$\alpha_x, M\|\|[100]$	$\alpha_z, M\|\|[001]$	T_c (K)
TiMnP	6.15	3.47	7.20	1.74	—	624	—	224	−2.08	0.02	420
ZrMnP	6.43	3.63	7.51	2.06	1.80 [37]	962	1000 [37]	778	0.21	−3.43	545
HfMnP	6.37	3.60	7.45	1.95	2.00 [37]	1516	1500 [37]	769	0.01	−2.97	550

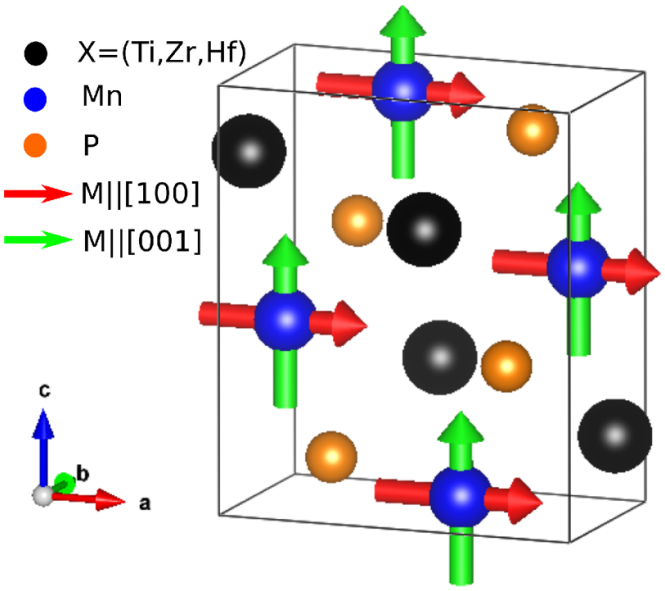

Figure 1. Crystal structure of XMnP (X = Ti,Zr,Hf) with magnetic moments of Mn atoms pointing along [100]-direction (red) and along [001]-direction (green).

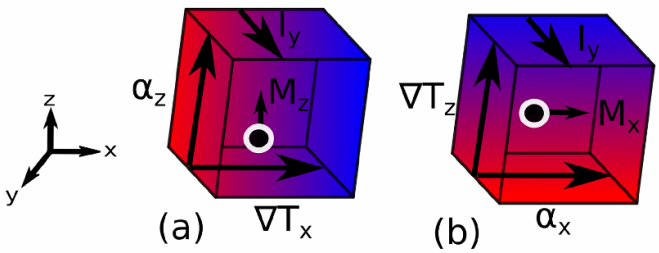

Figure 2. Schematic illustration of the induced anomalous Nernst conductivity direction change for (a) magnetization direction parallel to [001] axis (b) magnetization direction parallel to [100] axis.

same principles apply to AHC with the electric field replacing the thermal gradient, demonstrating the geometry in which the induced AHC/ANC is parallel to the magnetization. An interesting question is weather the AHC and ANC vectors of the XMnP (X = Ti,Zr,Hf) compounds of the MM′X family are modified by altering the magnetization direction. In order to address, we calculated AHC and ANC for the magnetization direction being along [100] and [001], as illustrated in figure 1. An increase of AHC with changing the magnetization direction from [001] to [100] is observed in all compounds. Namely, for TiMnP there is an almost three times increase (from 224 S cm^{-1} with $M||[001]$ to 624 S cm^{-1} with $M||[100]$). More interestingly, the calculated value of 778 S cm^{-1} with $M||[001]$ jumps to 962 S cm^{-1} with $M||[100]$ in ZrMnP and the 769 S cm^{-1} with $M||[001]$ skyrockets to 1516 S cm^{-1} with $M||[100]$ for HfMnP, being in excellent agreement with the reported theoretical (experimental) values of 1000 S cm^{-1} (900 S cm^{-1}) and 1500 S cm^{-1} (1400 S cm^{-1}) for ZrMnP and HfMnP respectively [37], calculated for $M||[100]$, as shown in figure 4(b) and table 1. It is further noted that the calculated value of AHC of HfMnP is larger than many compounds discussed in [53] including the reported value of −1310 S cm^{-1} for $Co_3Sn_2S_2$ in [54] and many Heusler compounds reported in [55].

Surprisingly, the calculated ANC exhibits a peculiar behavior, where for TiMnP the finite value of −2.08 A mK^{-1} for the [100] direction becomes 0.02 A mK^{-1} for the [001] direction. The opposite behavior is observed in HfMnP and ZrMnP where the small values of 0.21 A mK^{-1} and 0.01 A mK^{-1} respectively increase (in absolute value) to −2.97 A mK^{-1} and −3.43 A mK^{-1}, which is among the largest reported in [54]. Similar ANC changes have been studied in non-collinear antiperovkites in [56]. These discrepant AHC/ANC values serve an interesting playground for AHC/ANC manipulations by altering the magnetization direction of the compounds, as illustrated in figure 2, that can be useful for transverse thermoelectric generation having great potential for energy harvesting and heat sensing applications [57–61].

To estimate the Curie temperatures (T_c) we calculate the magnetic exchange interactions (J_{ij}) using the Liechtenstein formula [62] as implemented in the juKKR code [63] using Perdew Burke Ernzerhof (PBE) and full-potential approximation (see figure 3(a)). The T_cs were then calculated using Metropolis Monte Carlo method to solve the Heisenberg model, and the values taken from the Binder cumulant. All three simulated compounds show ferromagnetic behavior and finite temperatures as shown in figure 3(b), all T_c values were larger than room temperature, being 420, 545, 550 K for TiMnP ZrMnP and HfMnP respectively. This is attested by the strong ferromagnetic (positive J_{ij}) interactions between Mn–Mn in the nearest and next-nearest neighbors, with subsequent interactions also being mostly FM in nature.

It is observed that the symmetry of the Berry curvature plays the predominant role in determining the numerical values of the AHC and ANC tensor elements, given by equations (1) and (3) respectively. Since the Berry curvature

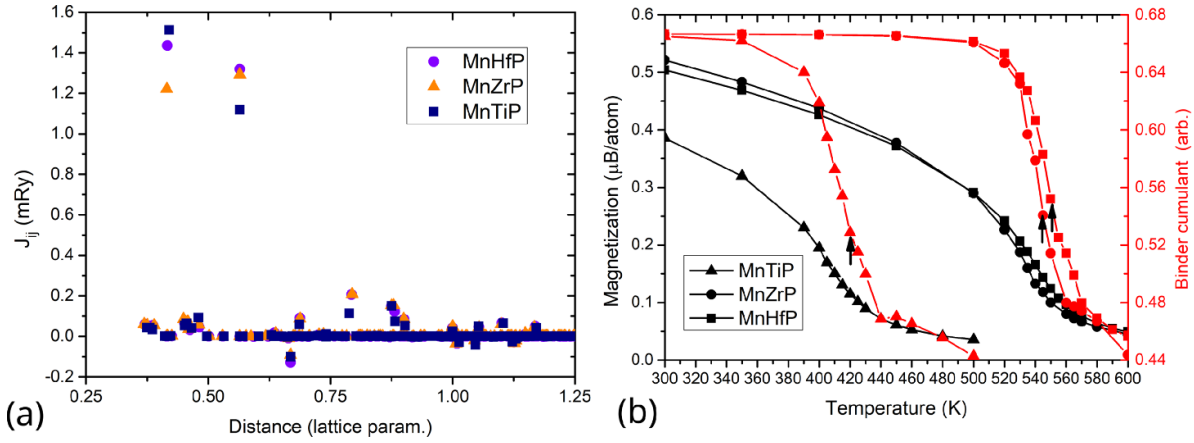

Figure 3. Exchange interactions (J_{ij}) as a function of distance (a) to evaluate the T_c (b).

behaves as a pseudovector under symmetry operations, it is possible to predetermine its value based on the magnetic point group of the compound, according to the formula [64]:

$$s\mathbf{\Omega}(\mathbf{k}) = \pm det(\mathbf{D}(R))\,\mathbf{D}(R)\,\mathbf{\Omega}\left(s^{-1}\mathbf{k}\right), \tag{4}$$

where $\mathbf{\Omega}(r)$ denotes the pseudovector Berry curvature, $\mathbf{D}(R)$ the three-dimensional matrix representation of a symmetry operator without the translation part and finally s the matrix representation of an arbitrary symmetry operation. The underlying compounds of XMnP (X = Ti,Zr,Hf) with the magnetization direction parallel to [100]-axis, belong to the magnetic space group $Pnm'a'$ (62.447), in which the presence of 2_{100} symmetry operation, after summing over all Brillouin zone, forces $\Omega_y = \Omega_z = 0$, following the relations:

$$\begin{aligned}
\Omega_x(k_x,-k_y,-k_z) &= \Omega_x(k_x,k_y,k_z),\\
\Omega_y(k_x,-k_y,-k_z) &= -\Omega_y(k_x,k_y,k_z),\\
\Omega_z(k_x,-k_y,-k_z) &= -\Omega_x(k_x,k_y,k_z).
\end{aligned} \tag{5}$$

On the other hand there is no condition implying vanishing value for Ω_x, meaning that σ_x is allowed to have finite value, as it happens. By changing the magnetization direction parallel to [001]-axis, the resulting magnetic space group alters to $Pn'm'a$ (62.446), in which the presence of 2_{001} leads to $\Omega_x = \Omega_y = 0$ and leaving Ω_z unrestricted, after summing over all Brillouin zone, according to:

$$\begin{aligned}
\Omega_x(-k_x,-k_y,k_z) &= -\Omega_x(k_x,k_y,k_z),\\
\Omega_y(-k_x,-k_y,k_z) &= -\Omega_y(k_x,k_y,k_z),\\
\Omega_z(-k_x,-k_y,k_z) &= \Omega_z(k_x,k_y,k_z).
\end{aligned} \tag{6}$$

Since the AHC depends on the Berry curvature, according to equation (1), its corresponding tensors for the different orientations of the magnetization are summarized in table 2. It is noted that the absence of symmetry operations forcing a specific component to vanish, does not necessarily guarantee its finite value, as it was found for Co_2NbAl in [53].

Negligible ANC values are allowed even in the presence of finite AHC values evaluated at the Fermi energy. The shape of the AHC tensor is determined by the Berry curvature, as

Table 2. AHC tensors for different magnetic space groups.

AHC tensor for Pnm′a′ (BNS: 62.446) **M**‖ [100]	AHC tensor for Pn′m′a (BNS: 62.446) **M**‖ [001]
$\sigma = \begin{pmatrix} 0 & 0 & 0 \\ 0 & 0 & \sigma_x \\ 0 & -\sigma_x & 0 \end{pmatrix}$	$\sigma = \begin{pmatrix} 0 & \sigma_z & 0 \\ -\sigma_z & 0 & 0 \\ 0 & 0 & 0 \end{pmatrix}$

described by equation (4). The same principles apply to the ANC tensor therefore one would expect the same non vanishing components in both AHC and ANC tensors. While this is in principle true, there are certain conditions in which the ANC exhibits an incidental vanishing value in the presence of a finite AHC value. The first, trivial case, appears when the AHC is a finite constant for a wide range of energies around the Fermi energy. In this case, the derivative of a constant vanishes, giving negligible ANC values, as occurs in TiMnP for magnetization parallel to [001]-axis (see blue AHC curve in figure 4(b) and the resulting blue ANC curve in figure 4(d)). Another, less obvious, case happens if the AHC curve as a function of energy is symmetric (or almost symmetric) for a certain range around the Fermi energy. In this case, the contribution from the range below the Fermi energy will cancel out the one from the range above the Fermi energy, giving rise to vanishing ANC value, as observed in HfMnP for magnetization parallel to [100]-axis (see black AHC curve in figure 4(a) and the resulting black ANC curve in figure 4(c)).

The AHC exhibits a disperse nature originating from the whole Brillouin zone. In order to identify the regions of dominant AHC contribution, we split the Brillouin zone of each of the underlying MM′X compounds, with magnetization direction fixed along [100]-direction, in $6 \times 6 \times 6$ cubes, within each of which the σ_x component of the AHC tensor was calculated. The results are illustrated in figures 5(a)–(c) for TiMnP, ZrMnP and HfMnP respectively. We observe that the hot spot contributions in figures 5(b) and (c) correspond to nodal lines in figures 6(d)–(f) and (g)–(i) for (Zr,Hf)MnP respectively, in complete agreement with [37]. Unlike the other two compounds, a direct comparison of figure 5(a) with

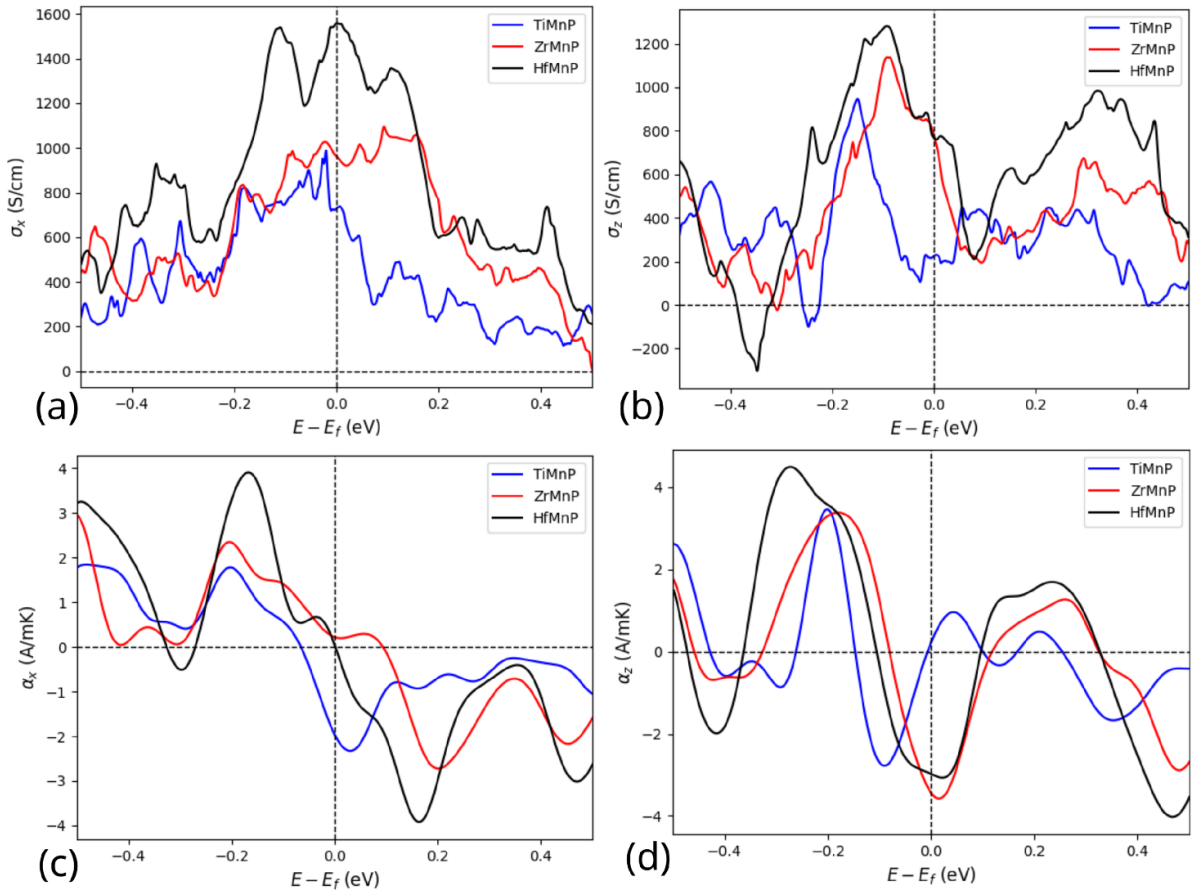

Figure 4. (a) σ_x for XMnP (X = Ti,Zr,Hf) with magnetization direction parallel to [100]-axis. (b) σ_z for XMnP (X = Ti,Zr,Hf) with magnetization direction parallel to [001]-axis. (c) α_x for XMnP (X = Ti,Zr,Hf) with magnetization direction parallel to [100]-axis. (d) α_z for XMnP (X = Ti,Zr,Hf) with magnetization direction parallel to [001]-axis.

figures 6(a)–(c) for TiMnP, reveals the presence of several nodal lines as the main origin of the enhanced AHC for the range $k_z \in (0.00, 0.33)$, however, small gap areas that contribute, alongside nodal lines, are found within the range $(k_x, k_y) \in (0.00, 0.16)$, $k_z\,(0.33, 0.500)$ of figure 6(c). That is, for TiMnP the total AHC value originates from a combination of nodal lines and small gap areas. Discrepant neighboring AHC values affect the ANC that is calculated in a similar way by integrating the AHC within the specified limit of each cube, as shown in figures 5(d)–(f). Similarly, the contribution originates from a wide range of Brillouin zone.

Large changes of AHC & ANC values calculated for the different magnetization directions can occur even in the absence of localized contributions. Since altering the magnetization direction affects the finite AHC component, based on the geometry of figure 2, the calculated AHC changes reflect the AHC vector. Our calculations verify an increase of 441 S cm^{-1}, 182 S cm^{-1} and 693 S cm^{-1} in the AHC vector when the magnetization is altered from [001]-axis to [100]-axis for XMnP (X = Ti,Zr,Hf) respectively. Therefore, one interesting question is whether, by tuning the magnetization direction, there are emerging localized contributions originating from weyl nodes that compose the main difference in the calculated values or not. In order to identify the origin of the main difference, we split the Brillouin zone in 50 parallelepipeds for $k_z \in [0.0, 0.50]$ and compute the AHC & ANC vector change within (see figure 7). It is highlighted that, for all compounds, even though there are notable differences among the contributions of several k_z ranges, there is no dominant contribution, resulting in the almost uniform distribution of figures 7(a)–(f). As a result, it is demonstrated that large AHC and ANC differences are originating from small changes throughout the whole Brillouin zone instead of gigantic localized contributions.

What affects the AHC sign? Comparing the distribution of σ_x component in all MM′X compounds, illustrated in figures 5(a)–(c), we came across an interesting observation. The strong disperse negative-sign area of TiMnP within the rectangle $(k_x, k_y) \in [-0.166, 0.166], k_z \in [0.333, 0.500]$ (see figure 5(a)) does not exist in any of the other compounds. In order to investigate the origin of this contribution, explicit band structure search was performed, revealing that the presence of a nodal line at the spatial vicinity of $(k_x, k_y) \approx 0.03, k_z \in [0.420, 0.500]$ is responsible for this enhanced value, by contributing (including the symmetry equivalent parts) 5.6% (35 S cm^{-1} out of 624 S cm^{-1}) to the total value.

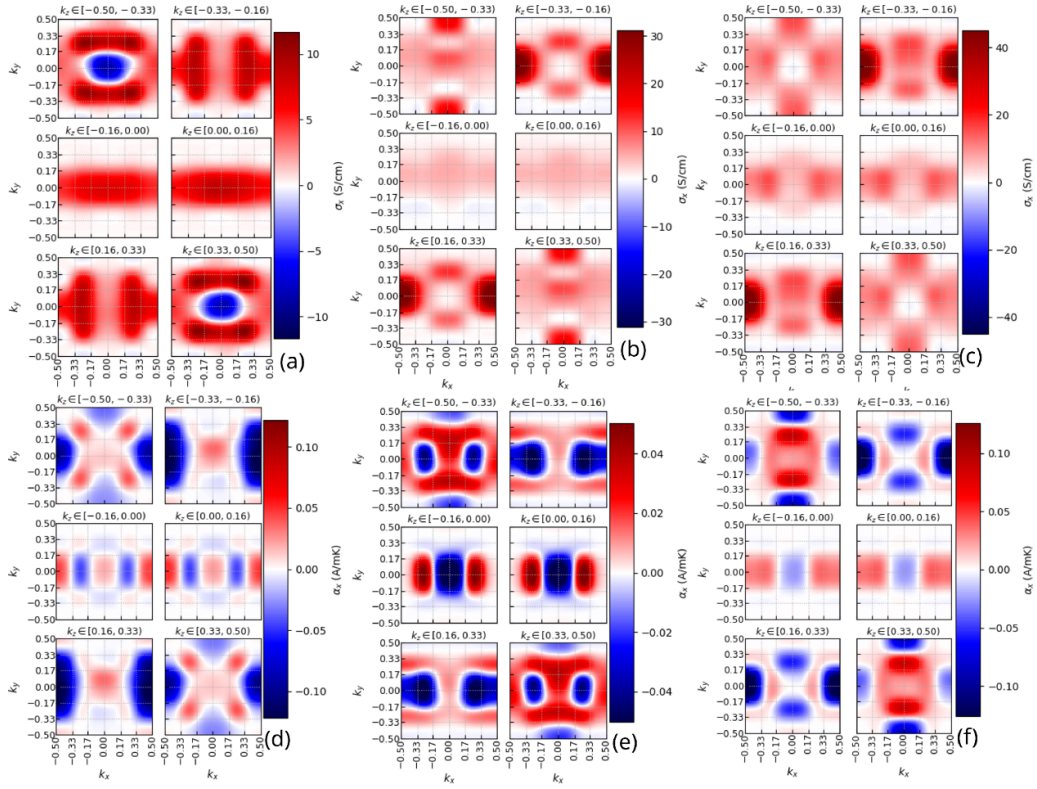

Figure 5. The x-component of AHC (σ_x) and ANC (α_x) evaluated within 216 cubes in the whole Brillouin zone for XMnP (X = Ti,Zr,Hf). (a) σ_x for TiMnP with $M||[100]$ (b) σ_x for ZrMnP with $M||[100]$ (c) σ_x for HfMnP with $M||[100]$ (d) α_x for TiMnP with $M||[100]$ (e) α_x for ZrMnP with $M||[100]$ (f) α_x for HfMnP with $M||[100]$.

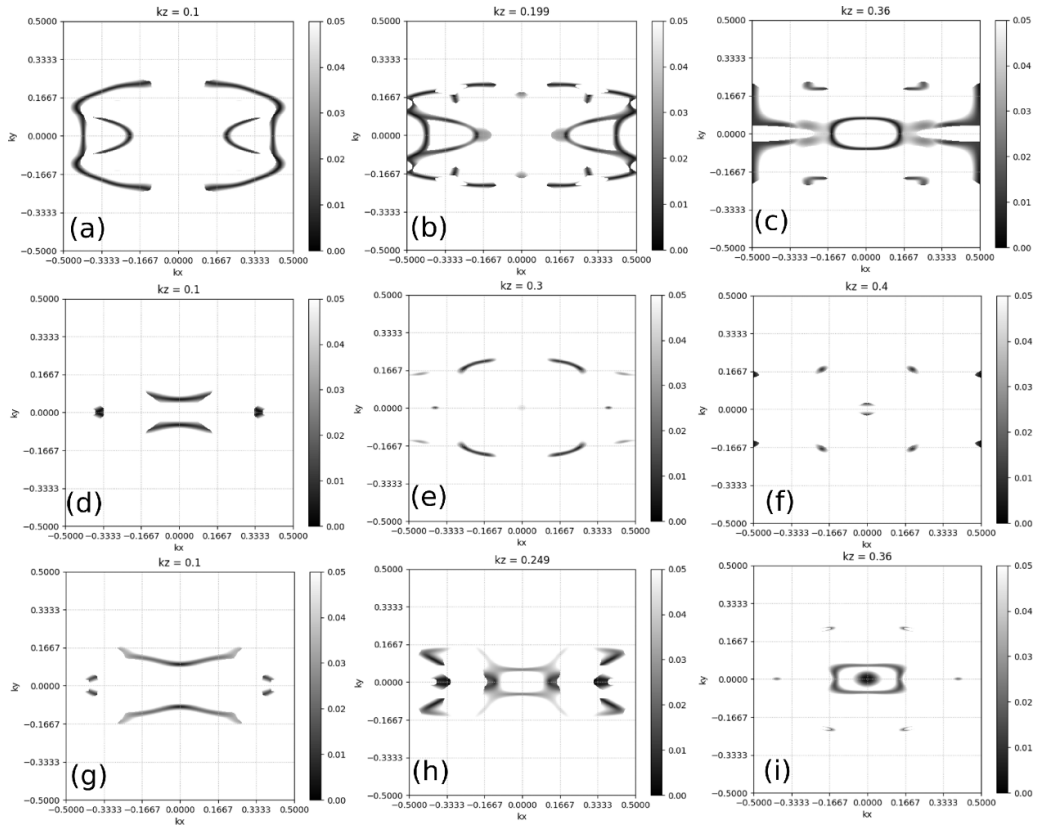

Figure 6. Gap of selected k_z slices of the Brillouin zone for TiMnP (a)–(c), ZrMnP (d)–(f) and HfMnP (g)–(i).

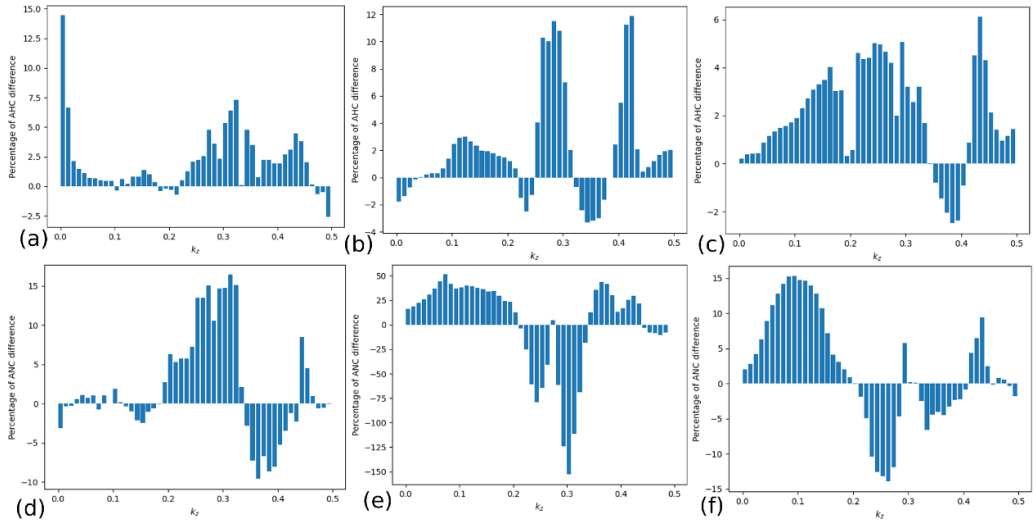

Figure 7. Percentage of AHC vector change between magnetization directions [001] and [100] for $k_z \in [0.00, 0.50]$ for (a) TiMnP, (b) ZrMnP, (c) HfMnP and ANC vector for (d) TiMnP (e) ZrMnP (f) HfMnP.

The reason of the negative sign contribution though is unclear and it might be an interesting topic for further research.

4. Conclusion

Using first principles calculations, we evaluated the AHC and ANC of XMnP (X = Ti,Zr,Hf) compounds of the MM′X family and altered the magnetization direction to tune such transport properties. The detailed symmetry analysis based on the magnetic point group of the compounds indicated the vanishing and finite values of AHC and ANC tensors, verifying the validity of our results. It is noted that altering the magnetization direction from [001] to [100]-axis, significantly affects the AHC & ANC values with their differences originating from band structure changes throughout the whole Brillouin zone. The observed AHC/ANC enhancements due to the change in the magnetization direction make an interesting opportunity for using materials susceptible to changing magnetization direction to transverse thermoelectric generation applications.

Data availability statement

The data that support the findings of this study are available upon reasonable request from the authors.

Acknowledgments

This work was financially supported by the Deutsche Forschungsgemeinschaft (DFG) via the priority programme SPP 1666 and the calculations were conducted on the Lichtenberg high performance computer of the TU Darmstadt. We thank Dr Ruiwen Xie for valuable discussions.

ORCID iDs

Ilias Samathrakis https://orcid.org/0000-0001-9754-145X
Chen Shen https://orcid.org/0000-0002-8538-9873
Hongbin Zhang https://orcid.org/0000-0002-1035-8861

References

[1] Žutić I, Fabian J and Sarma S D 2004 *Rev. Mod. Phys.* **76** 323
[2] Nagaosa N, Sinova J, Onoda S, MacDonald A H and Ong N P 2010 *Rev. Mod. Phys.* **82** 1539
[3] Behnia K and Aubin H 2016 *Rep. Prog. Phys.* **79** 046502
[4] Lee W L, Watauchi S, Miller V, Cava R and Ong N 2004 *Phys. Rev. Lett.* **93** 226601
[5] Chen H, Niu Q and MacDonald A H 2014 *Phys. Rev. Lett.* **112** 017205
[6] Zhang Y, Železny J, Sun Y, Van Den Brink J and Yan B 2018 *New J. Phys.* **20** 073028
[7] Nayak A K *et al* 2016 *Sci. Adv.* **2** e1501870
[8] Ganguly S, Costa M, Klautau A B, Bergman A, Sanyal B, Mookerjee A and Eriksson O 2011 *Phys. Rev.* B **83** 094407
[9] Yang H, Sun Y, Zhang Y, Shi W J, Parkin S S and Yan B 2017 *New J. Phys.* **19** 015008
[10] Kübler J and Felser C 2014 *Europhys. Lett.* **108** 67001
[11] Li X, Xu L, Ding L, Wang J, Shen M, Lu X, Zhu Z and Behnia K 2017 *Phys. Rev. Lett.* **119** 056601
[12] Guo G Y and Wang T C 2017 *Phys. Rev.* B **96** 224415
[13] Kiyohara N, Tomita T and Nakatsuji S 2016 *Phys. Rev. Appl.* **5** 064009
[14] Ikhlas M, Tomita T, Koretsune T, Suzuki M T, Nishio-Hamane D, Arita R, Otani Y and Nakatsuji S 2017 *Nat. Phys.* **13** 1085–90
[15] Železny J, Zhang Y, Felser C and Yan B 2017 *Phys. Rev. Lett.* **119** 187204
[16] Zhou X, Hanke J P, Feng W, Blügel S, Mokrousov Y and Yao Y 2020 *Phys. Rev. Mater.* **4** 024408
[17] Gurung G, Shao D F, Paudel T R and Tsymbal E Y 2019 *Phys. Rev. Mater.* **3** 044409
[18] Huyen V T N, Suzuki M T, Yamauchi K and Oguchi T 2019 *Phys. Rev.* B **100** 094426
[19] Feng Z, *et al* 2020 arXiv:2002.08712

[20] Hasegawa K, Mizuguchi M, Sakuraba Y, Kamada T, Kojima T, Kubota T, Mizukami S, Miyazaki T and Takanashi K 2015 *Appl. Phys. Lett.* **106** 252405
[21] Huang S, Wang W, Lee S, Kwo J and Chien C 2011 *Phys. Rev. Lett.* **107** 216604
[22] Johnson V 1975 *Inorg. Chem.* **14** 1117–20
[23] Szytula A, Pedziwiatr A, Tomkowicz Z and Bazela W 1981 *J. Magn. Magn. Mater.* **25** 176–86
[24] Jeitschko W 1975 *Acta Crystallogr.* B **31** 1187–90
[25] Yu S, Liu Z, Liu G, Chen J, Cao Z, Wu G, Zhang B and Zhang X 2006 *Appl. Phys. Lett.* **89** 162503
[26] Barandiarán J, Chernenko V, Lázpita P, Gutiérrez J and Feuchtwanger J 2009 *Phys. Rev.* B **80** 104404
[27] Ullakko K, Huang J, Kantner C, O'handley R and Kokorin V 1996 *Appl. Phys. Lett.* **69** 1966–8
[28] Wu G, Yu C, Meng L, Chen J, Yang F, Qi S, Zhan W, Wang Z, Zheng Y and Zhao L 1999 *Appl. Phys. Lett.* **75** 2990–2
[29] Kainuma R *et al* 2006 *Nature* **439** 957–60
[30] Krenke T, Duman E, Acet M, Wassermann E F, Moya X, Mañosa L and Planes A 2005 *Nat. Mater.* **4** 450–4
[31] Gutfleisch O, Willard M A, Brück E, Chen C H, Sankar S and Liu J P 2011 *Adv. Mater.* **23** 821–42
[32] Tegus O, Brück E, Buschow K and De Boer F 2002 *Nature* **415** 150–2
[33] Liu J, Gottschall T, Skokov K P, Moore J D and Gutfleisch O 2012 *Nat. Mater.* **11** 620–6
[34] Liu E *et al* 2013 *Appl. Phys. Lett.* **102** 122405
[35] Glanz J 1998 *Science* **279** 2045
[36] GschneidnerJr K A, Pecharsky V and Tsokol A 2005 *Rep. Prog. Phys.* **68** 1479
[37] Singh S, Noky J, Bhattacharya S, Vir P, Sun Y, Kumar N, Felser C and Shekhar C 2021 *Adv. Mater.* **33** 2104126
[38] Lamichhane T N, Taufour V, Masters M W, Parker D S, Kaluarachchi U S, Thimmaiah S, Bud'ko S L and Canfield P C 2016 *Appl. Phys. Lett.* **109** 092402
[39] Weischenberg J, Freimuth F, Sinova J, Blügel S and Mokrousov Y 2011 *Phys. Rev. Lett.* **107** 106601
[40] Zimmermann B *et al* 2014 *Phys. Rev.* B **90** 220403
[41] Tian Y, Ye L and Jin X 2009 *Phys. Rev. Lett.* **103** 087206
[42] Kresse G and Hafner J 1993 *Phys. Rev.* B **47** 558
[43] Perdew J P, Burke K and Ernzerhof M 1996 *Phys. Rev. Lett.* **77** 3865
[44] Mostofi A A, Yates J R, Lee Y S, Souza I, Vanderbilt D and Marzari N 2008 *Comput. Phys. Commun.* **178** 685–99
[45] Zhang Z, Zhang R W, Li X, Koepernik K, Yao Y and Zhang H 2018 *J. Phys. Chem. Lett.* **9** 6224–31
[46] Wu Q, Zhang S, Song H F, Troyer M and Soluyanov A A 2018 *Comput. Phys. Commun.* **224** 405–16
[47] Xiao D, Chang M C and Niu Q 2010 *Rev. Mod. Phys.* **82** 1959–2007
[48] Liu X *et al* 2004 *Physica* E **20** 370–3
[49] Chernyshov A, Overby M, Liu X, Furdyna J K, Lyanda-Geller Y and Rokhinson L P 2009 *Nat. Phys.* **5** 656–9
[50] Brataas A, Kent A D and Ohno H 2012 *Nat. Mater.* **11** 372–81
[51] Sasaki R, Nii Y and Onose Y 2021 *Nat. Commun.* **12** 1–7
[52] Hahn S *et al* 2019 *Nature* **570** 496–9
[53] Samathrakis I, Long T, Zhang Z, Singh H K and Zhang H 2021 *J. Phys. D: Appl. Phys.* **55** 074003
[54] Wang Q, Xu Y, Lou R, Liu Z, Li M, Huang Y, Shen D, Weng H, Wang S and Lei H 2018 *Nat. Commun.* **9** 1–8
[55] Noky J, Zhang Y, Gooth J, Felser C and Sun Y 2020 *npj Comput. Mater.* **6** 1–8
[56] Singh H K, Samathrakis I, Shen C and Zhang H 2022 *Phys. Rev. Mater.* **6** 045402
[57] Zhou W, Yamamoto K, Miura A, Iguchi R, Miura Y, Uchida K i and Sakuraba Y 2021 *Nat. Mater.* **20** 463–7
[58] Uchida K i, Zhou W and Sakuraba Y 2021 *Appl. Phys. Lett.* **118** 140504
[59] Sakai A *et al* 2020 *Nature* **581** 53–57
[60] Holanda J, Santos O A and Rezende S M 2021 *Phys. Rev. Appl.* **16** 014051
[61] Yamamoto K, Iguchi R, Miura A, Zhou W, Sakuraba Y, Miura Y and Uchida K i 2021 *J. Appl. Phys.* **129** 223908
[62] Liechtenstein A I, Katsnelson M, Antropov V and Gubanov V 1987 *J. Magn. Magn. Mater.* **67** 65–74
[63] Rüßmann P *et al* 2018 *J. Phys. Mater.* **1** 015002
[64] Seemann M, Ködderitzsch D, Wimmer S and Ebert H 2015 *Phys. Rev.* B **92** 155138